# The Yeast Mitochondrial Citrate Transport Protein: Determination of Secondary Structure and Solvent Accessibility of Transmembrane Domain IV Using Site-Directed Spin Labeling†

Ronald S. Kaplan,*,‡ June A. Mayor,‡ Rusudan Kotaria,‡ D. Eric Walters,‡ and Hassane S. Mchaourab*,§,||

*Department of Biochemistry & Molecular Biology, FUHS/The Chicago Medical School, 3333 Green Bay Road, North Chicago, Illinois 60064, and National Biomedical ESR Center, Biophysics Research Institute, Medical College of Wisconsin, 8701 Watertown Plank Road, Milwaukee, Wisconsin 53226*

*Received February 25, 2000; Revised Manuscript Received May 31, 2000*

ABSTRACT: To explore the spatial organization and functional dynamics of the citrate transport protein (CTP), a nitroxide scan was carried out along 22 consecutive residues within the fourth transmembrane domain (TMDIV). This domain has been implicated as being of unique importance to the CTP mechanism due to (i) the presence of two intramembranous positive charges that are essential for CTP function and (ii) the existence of a transmembrane aqueous surface within this domain which likely corresponds to a portion of the citrate translocation pathway. The sequence-specific variation in the mobilities of the introduced nitroxides and their accessibilities to molecular $O_2$ reveal an α-helical conformation along the sequence. The accessibilities to NiEDDA are out of phase with accessibilites to $O_2$, indicating that one face of the helix is solvated by the lipid bilayer while the other is solvated by an aqueous environment. A gradient of NiEDDA accessibility is observed along the helix surface facing the aqueous phase, and the EPR spectral line shapes at these sites indicate considerable motional restriction. In the context of the model where TMDIV lines the translocation pathway, these data suggest a barrier to passive diffusion through the pathway. This paper reports the first use of site-directed spin labeling to study mitochondrial transporter structure.

The mitochondrial citrate transport protein (i.e., CTP)[1] from higher eukaryotic organisms catalyzes the efflux of tricarboxylates plus a proton across the mitochondrial inner membrane in exchange for either another tricarboxylate-$H^+$, a dicarboxylate (i.e., malate, succinate), or phosphoenolpyruvate (*1*). Following diffusion through a pore protein (i.e., VDAC) in the outer mitochondrial membrane, the resulting cytoplasmic citrate provides carbon fuel for the sterol and the fatty acid biosynthetic pathways, as well as a supply of $NAD^+$ (via the sequential action of ATP-citrate lyase and malate dehydrogenase) for glycolysis (*2*−*5*). The function of CTP has been shown to be altered in type 1 diabetes (*6*) in a manner that can be corrected via administration of exogenous insulin (*7*). Because of the central role of CTP in intermediary metabolism, it has been extensively studied using genetic and biochemical approaches (*8*−*11*).

Recently, we identified the yeast homologue of the higher eukaryotic CTP (*12*). An advantage afforded by the yeast carrier is that, following overexpression and subsequent purification, its function can be reconstituted in a liposomal system with high specific activity. Thus, the yeast CTP represents ideal material for a comprehensive structure/function analysis. To this end, we have embarked upon an extensive program of site-directed mutagenesis combined with the use of biochemical and biophysical approaches in order to probe the structural basis underlying CTP function. A Cys-less CTP which displays functional properties nearly identical to those of the wild-type CTP has been constructed (*13*). Moreover, we have demonstrated that both the wild-type and the Cys-less CTPs exist as homodimers of a 32.2 kDa subunit (*14*). Hydropathy analysis indicates that each monomer is likely to contain six membrane-spanning domains. However, little is known concerning the spatial organization of the helices in the monomer and the assembly of the dimer. Similar to other membrane proteins, no general method exists for the crystallization of mitochondrial transporters. Consequently, the detailed mechanism of transport and the conformational dynamics involved have not been elucidated.

An alternative approach to determine protein folding patterns and their functional dynamics is through the systematic application of spin labeling electron paramagnetic resonance (i.e., EPR) (*15, 16*). In this technique, nitroxide reporter groups are site-specifically introduced into protein sequences via cysteine mutagenesis followed by reaction with

†This work was supported by National Institutes of Health Grants GM-54642 to R.S.K. and RR01008 to H.S.M.

* To whom correspondence should be addressed. R.S.K.: Tel 847-578-8840; Fax 847-578-3240; E-mail kaplanr@mis.finchcms.edu. H.S.M.: Tel 615-322-3307; Fax 615-322-7236; E-mail Hassane.Mchaourab@mcmail.vanderbilt.edu.

‡ FUHS/The Chicago Medical School.

§ Medical College of Wisconsin.

|| Present address: Department of Molecular Physiology and Biophysics, Vanderbilt University, 702 Light Hall, Nashville, TN 37232.

[1] Abbreviations: BTC, 1,2,3-benzenetricarboxylate; CTP, citrate transport protein; EPR, electron paramagnetic resonance; MTS, methanethiosulfonate; MTSEA, (2-aminoethyl)methanethiosulfonate hydrobromide; NiEDDA, nickel(II) ethylenediaminediacetate; SDSL, site-directed spin labeling; TMDIV, transmembrane domain IV.

10.1021/bi000433e CCC: $19.00 
Published on Web 07/13/2000

a sulfhydryl-specific spin label. EPR analysis of the spin labeled mutant protein results in a set of conformationally dependent parameters that describe the environment at the site of attachment. The nitroxide mobility and its solvent accessibility allow the structural classification of the site. The sequence-specific variations in these parameters allow the determination of secondary structure and protein topography. The relative orientation of secondary structure is then determined from internitroxide distance measurements in doubly labeled mutants. The efficacy of this approach has been demonstrated in both water-soluble proteins (*17*) and membrane proteins such as rhodopsin (*18*) and the lactose permease (*19, 20*).

Within the CTP, transmembrane domain IV (i.e., TMDIV), comprising residues 173 through 194, is of particular interest for several reasons. First, it contains two arginines which provide positive charge that is essential for CTP function (*13*). Second, using cysteine scanning mutagenesis in combination with chemical modification of single-Cys CTP variants with hydrophilic MTS reagents, we have demonstrated that modification of most of the engineered cysteines causes inhibition of transport (*21*). This finding demonstrates the importance of TMDIV in the substrate translocation mechanism, probably via its participation in the formation of a portion of the aqueous translocation pathway through the CTP.

In the present investigation we have utilized site-directed spin labeling to obtain a structural perspective on the role of TMDIV. The mobility of nitroxide side chains introduced at 22 consecutive residues in TMDIV and their accessibility to molecular $O_2$ and NiEDDA were measured. Our results indicate that TMDIV exists in an α-helical conformation. One face of the helix is solvated by the lipid bilayer while the other face is in contact with an aqueous medium that allows accessibility of the nitroxides to NiEDDA. If the water-accessible crevice formed by TMDIV in fact lines the translocation pathway, as has been suggested based on previous functional studies and accessibility data (*21*), then the presence of a gradient of decreased accessibility to NiEDDA is reflective of a barrier to passive diffusion. Consistent with such a model, EPR line shapes near the middle of the helix are immobilized, reflecting steric constraints on the nitroxide mobility.

## EXPERIMENTAL PROCEDURES

*Overexpression and Purification of Single-Cys CTP Mutants.* Single-Cys CTP mutants were constructed utilizing the Strategene QuikChange mutagenesis kit as previously described (*21*). The Cys-less CTP gene in pET-21a(+) served as the starting template. Each CTP mutant was overexpressed in *E. coli*, and the inclusion body fraction was isolated as previously detailed (*11, 12*). Mutant CTPs were solubilized from the inclusion body fraction with 1.2% sarkosyl (*12*). Following ultracentrifugation, the CTP mutants were stored at −80 °C. Each mutant was then purified as follows. Approximately 2.0 mL of thawed inclusion body extract was adsorbed to a MonoQ HR 5/5 column equilibrated with Buffer A (10 mM Tris-HCl, pH 7.6, + 0.3% sarkosyl). The column was sequentially washed in Buffer A and in Buffer A + 460 mM NaCl, and the CTP was then eluted in a shallow gradient of Buffer A + 460−550 mM NaCl. The eluate was analyzed by SDS−PAGE, and the most highly purified fractions were pooled and applied to a Sephacryl S-300 (26/60) column equilibrated in Buffer B (10 mM Tris-HCl, pH 7.6, 150 mM NaCl, 0.3% sarkosyl). The CTP eluted in a single symmetrical peak with an elution volume of approximately 150 mL. The CTP was then concentrated in a Millipore filter and stored at −80 °C.

Scheme 1

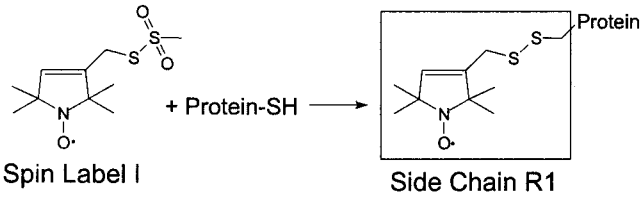


*Spin Labeling of CTP Mutants.* Single-Cys CTP mutants (approximately 15−25 nmol) were desalted using Micro Bio-Spin Columns (BioRad) which had been preequilibrated in 30 mM Hepes, 12.5 mM NaCl, 0.25 mM EDTA, 0.3% sarkosyl, pH 7.1. The CTP mutants were then incubated with a 10-fold molar excess of spin label I to generate side-chain R1 as shown in Scheme 1. The reaction was allowed to proceed for 2 h at room temperature in the dark. An additional 5-fold molar excess of label was then added and the reaction allowed to proceed for 3 more h. Each reaction mix was desalted twice on the Biospin columns, and the CTP was incorporated into phospholipid vesicles via the freeze−thaw−sonication technique as previously described (*8, 12*). Following a probe sonication step, the liposomes were chromatographed on Dowex in Buffer C (120 mM Hepes, 50 mM NaCl, 1 mM EDTA, pH 6.9), diluted in Buffer C (pH 7.1), and pelleted by ultracentrifugation at 314000*g*(max) for 45 min at 6 °C. The pellet was rinsed in Buffer C (pH 7.1), subjected to another ultracentrifugation, and then resuspended by gentle mixing in a minimal volume of Buffer C. Samples were stored at 4 °C prior to spectroscopic analysis.

*EPR Measurements.* EPR spectra were recorded at room temperature on a Varian 102 spectrometer fitted with a loop-gap resonator using 2 mW incident microwave power and 1.6 G field modulation. Power saturation measurements were carried out under a nitrogen atmosphere, in the presence of $O_2$ in equilibrium with air and in the presence of 70 mM NiEDDA in equilibrium with nitrogen. The data were analyzed to obtain the EPR accessibility parameter as previously described (*22*).

*Miscellaneous.* SDS−polyacrylamide gel electrophoresis was performed in precast 14% polyacrylamide Tris−glycine gels, and protein was stained with Coomassie Blue according to the manufacturer's (Novex) instructions. Protein was quantified utilizing the Amido Black method of Kaplan and Pedersen (*23*). Reconstituted BTC-sensitive [$^{14}$C]citrate/citrate exchange was determined exactly as described previously (*21*).

## RESULTS AND DISCUSSION

*Characterization of the Mutants.* Figure 1 shows a two-dimensional model of the CTP depicting the six transmembrane segments predicted from hydropathy analysis. Transmembrane domain IV, the subject of the present investigation, is highlighted. We have previously demonstrated (*21*) that upon overexpression in *E. coli*, solubilization, and subsequent

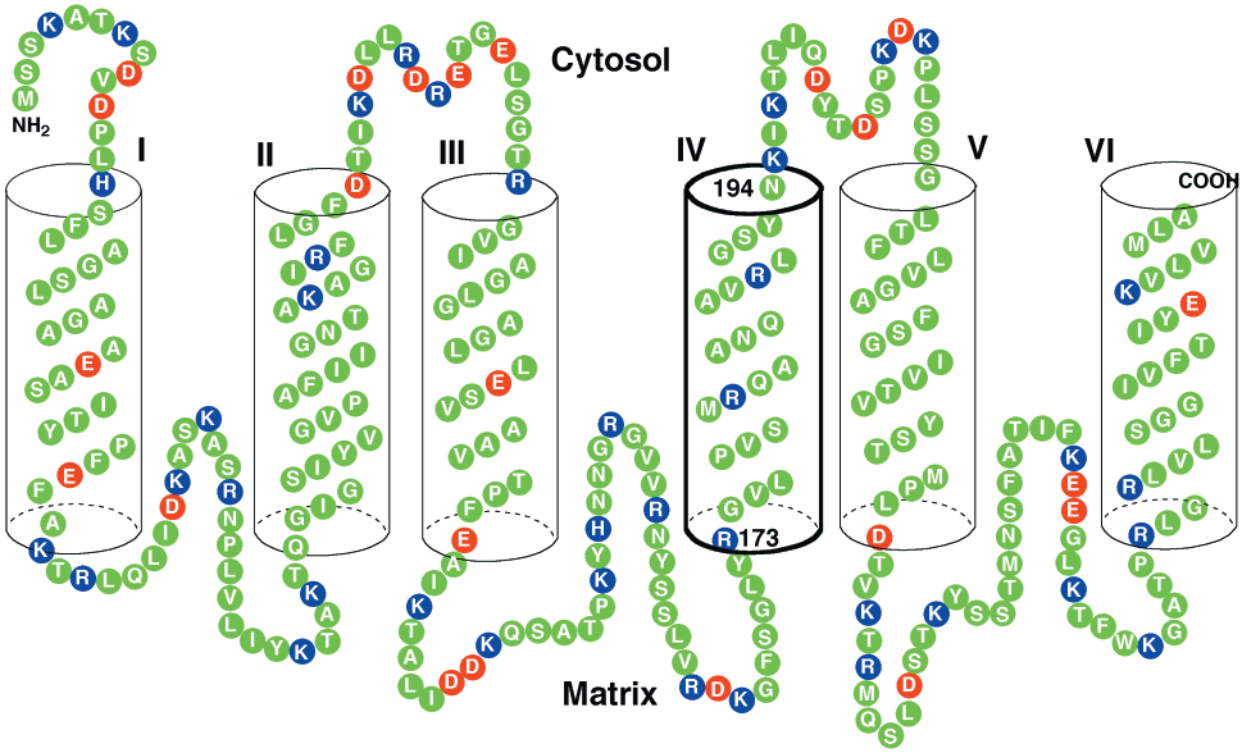


FIGURE 1: Schematic representation of the proposed membrane topology of the Cys-less yeast mitochondrial citrate transport protein monomer. Transmembrane domain IV, the subject of the present investigations, is highlighted. Positively charged residues (Arg, Lys, His) are depicted in blue and negatively charged residues (Asp, Glu) in red. Residues 173−194 were spin labeled as described in the text.

incorporation into liposomes, all cysteine variants of TMDIV retained significant BTC-sensitive citrate transport activity (i.e., the defining function of the mitochondrial citrate carrier), with the exception of the R181C and R189C mutants. Interestingly, chemical modification of the latter two mutants with MTSEA, a reagent that restores positive charge at these sites, partially restored CTP function (*13*). In summary, our previous work verifies that, with the possible exception of the R181C and R189C mutants, the structural and functional integrity of the CTP is preserved in this panel of single-Cys mutants.

In the present study, a nitroxide was introduced at each of 22 sites within transmembrane domain IV encompassing residues 173−194. Figure 2 depicts an SDS−PAGE profile of the Cys-less CTP and a representative set of single-Cys CTP mutants after reaction with spin label I (see Scheme 1) and subsequent desalting steps, immediately prior to incorporation into phospholipid vesicles. The gel lanes are overloaded with protein in order to reveal purity. As is evident from Figure 2, the labeling is carried out with highly purified preparations of each CTP variant. Densitometric analysis (of gels loaded with more moderate quantities of each preparation) indicates a mean purity of 93% ± 2% (SD).

Following attachment of R1, the reconstituted citrate transport activities obtained with the same subset of mutants are reported in Table 1. Based on hydropathy analysis, this representative set includes residues on both faces of the putative helix. For comparison, previously reported values (*21*) obtained in the absence of labeling are included. It is noteworthy that the introduction of R1 at sites 178, 182, 185, and 186 completely block transport. Based on both our previous MTS reactivity studies (*21*) as well as the present EPR studies described below, these residues are thought to

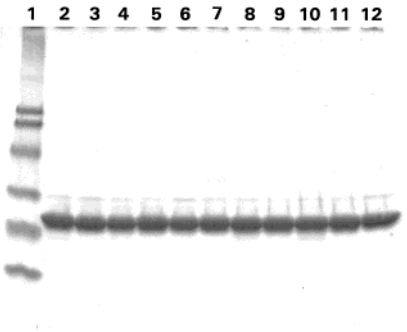


FIGURE 2: Coomassie-stained SDS−polyacrylamide gel depicting the purity of the Cys-less and single-Cys CTP mutants following purification, and labeling with spin label I. Proteins were electrophoresed on a precast 14% polyacrylamide gel (Novex) using the Tris−glycine buffer system. Lane 1, 8 μL of Bio-Rad prestained SDS−PAGE standards: phosphorylase B (106 000), bovine serum albumin (77 000), ovalbumin (50 800), carbonic anhydrase (35 600), soybean trypsin inhibitor (28 100), and lysozyme (20 900). Lane 2, 6 μg of the Cys-less CTP. Lanes 3−12, 6 μg of V178C, S179C, M180C, Q182C, A183C, N185C, Q186C, A187C, V188C, and L190C single-Cys CTP variants, respectively. Each CTP variant was purified, labeled with spin label I, and desalted prior to the electrophoresis, as described under Experimental Procedures.

face the aqueous translocation pathway and/or other portions of the protein (e.g., see Figure 5). We postulate that the inhibition is a consequence of a direct steric block of the citrate translocation pathway by the spin label, thereby preventing substrate permeation. Consistent with this hypothesis is the finding that the molecular dimensions of R1

Table 1: Effect of Spin Labeling on Reconstituted Function of Single-Cys CTP Mutants

| | reconstituted specific transport activity[a] | |
|---|---|---|
| mutation | prior to spin labeling (%)[b] | following spin labeling (%)[c] |
| Cys-less | 100 | 100 |
| V178C | 109 | 1 |
| S179C | 166 | 82 |
| M180C | 23 | 22 |
| Q182C | 3 | 1 |
| A183C | 129 | 71 |
| N185C | 60 | 1 |
| Q186C | 16 | 2 |
| A187C | 163 | 53 |
| V188C | 68 | 26 |
| L190C | 43 | 18 |

[a] Overexpressed, solubilized, single-Cys CTP mutants were incorporated into phospholipid vesicles. Transport incubations were conducted at room temperature, and the BTC-sensitive [$^{14}$C]citrate/citrate exchange was measured. Percentages were calculated by comparison to the Cys-less CTP values. [b] Data were recalculated from ref *21*. In the absence of labeling with spin label I, the Cys-less CTP displayed a reconstituted specific transport activity of 758 nmol min$^{-1}$ (mg of protein)$^{-1}$. [c] Following labeling with spin label I and subsequent desalting, the reconstituted Cys-less CTP displayed a specific transport activity of 633 nmol min$^{-1}$ (mg of protein)$^{-1}$.

are slightly greater than those of citrate (e.g., the van der Waals surface of R1 can be contained in a cylinder with a length of 9.3 Å and a diameter of 9.0 Å; the comparable dimensions for citrate are 10.4 Å × 7.2 Å). It is interesting that spin labeling of position 190, a site that is thought to face the translocation pathway, only partially inhibits transport. It is possible that as the external surface of the bilayer is approached, greater conformational flexibility exists, such that the steric block by the spin label is less pronounced.

In contrast, R1 substitution at sites which, based on MTS reactivity studies, are thought to face the lipid bilayer (i.e., 179, 180, 183, 187, 188) is much less disruptive of CTP function. This is not unexpected considering the relative hydrophobicity of R1 and its high helical propensity (*24, 25*). Furthermore, this result suggests that the loss of function detected at the water-exposed face of the helix is not a consequence of a structural perturbation intrinsic to the nitroxide side-chain itself, but instead likely originates from the steric mechanism described above. In fact, previous studies with bacteriorhodopsin, rhodopsin, and lac permease suggest that R1 can be introduced at membrane-exposed helix surfaces with minimal destabilization of the structure (*15, 19, 26, 27*). It is noted that charged MTS reagents completely abolished transport activity when introduced at the same sites in CTP (*21*).

*Mobility of R1 along TMDIV*. Figure 3 shows the room temperature EPR spectra of side-chain R1 at sites 173 through 194 in the fourth transmembrane segment of the CTP. In all the spectra, a sharp component, indicated by an arrow and labeled "F" in the spectrum of 185, is observed. This component was observed in a control preparation of the Cys-less CTP and presumably is due to contaminant proteins comprising approximately 5% of the Sephacryl-purified CTP. Experiments performed with the sarkosyl-solubilized Cys-less CTP indicate that on a spin basis this signal is at least 5-fold smaller than the signal obtained from an equivalent amount of single cysteine mutants.

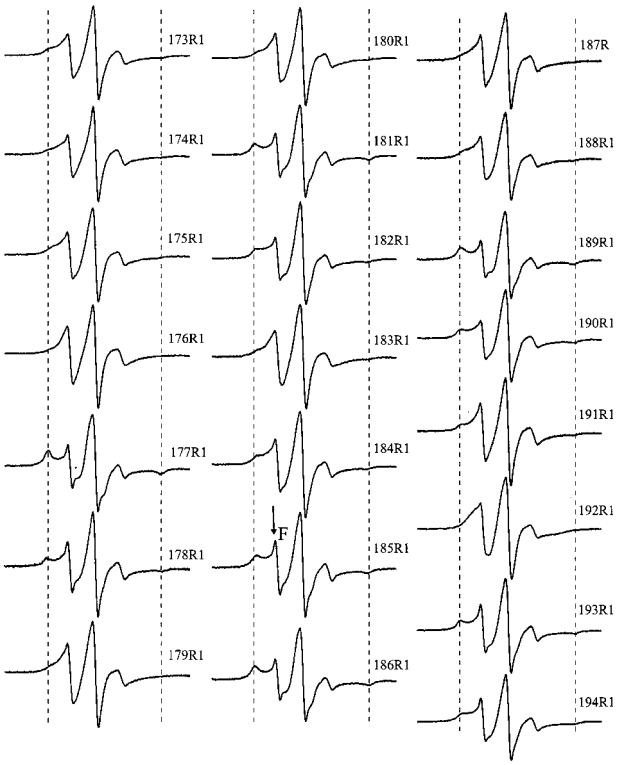


FIGURE 3: Room-temperature EPR spectra of R1-labeled single-Cys CTP mutants along TMDIV. The background spectral component is indicated by the arrow and the "F" in the 185R1 spectrum. The vertical dashed lines are to mark the location of the outer hyperfine extrema.

The line shapes in the spectra of the mutants report on dynamic modes that average the anisotropic **A** and **g** tensors. The largest contribution for side-chain R1 arises from rotational isomerization around the last two bonds that tether the nitroxide ring to the linking arm (*28*). Large-amplitude, local backbone fluctuations, particularly at exposed sites in loops, have also been proposed to contribute to the averaging of the magnetic tensors of R1 (*28, 29*). The mobility of the side-chain R1 is a general term that refers to the effectiveness of the various dynamic modes in averaging the tensors. Measures of mobilities include the rotational correlation time (*30*), the width of the central line, and the spectral second moment (*28*). While these measurements are coarse and phenomenological, they allow the classification of the structural class of each site, and their sequence-specific variation can be used to identify secondary structural elements (*28*).

Three distinct types of structural classes can be assigned based on mobility (*28*). The first class consists of sites where the spectral line shape indicates rapid and large-amplitude motions. These sites occur generally in loops or at the solvent-exposed surfaces of helices where R1 is not in contact with the protein tertiary structure. Qualitative analysis of the spectra in Figure 3 indicates that residues 176, 179, 180, 183, 187, 188, and 192 belong to this class. In contrast, the line shapes at residues in the second category, consisting of residues 177, 178, 181, 185, 186, 189, and 193, are characterized by the presence of resolved outer splittings indicating partial averaging of the **A** tensor. The broad central line is also consistent with partial averaging of the **g** tensor. These spectral characteristics are indicative of extensive

contacts of R1 in the tertiary structure. EPR spectral line shapes of the first and second type occur periodically along the sequence every third or fourth residue, suggesting a helical structure. An intermediate degree of averaging occurs at sites in the third category consisting of residues 173, 174, 175, 182, 184, 190, 191, and 194. The line shapes at these residues are characterized by increased intensities between the low-field peak and the central line and an inside shift in the position of the outer extrema. This type of two-component spectrum can also occur for R1 at exposed sites. There are two means to resolve this degeneracy. The first is the use of nitroxide side chains with different linking arms (*31*). The second is to determine the accessibility of R1 at these sites to polar and nonpolar reagents.

Another notable feature in the spectral set is the absence of evidence of spin−spin interactions. While the presence of background signal can obscure an intermediate level of spin−spin interactions, if TMDIV was along the dimer interface, short-range spin−spin interactions would have resulted in a distinct spectral feature flanking the low-field extremum (*32*).

*Accessibility and Secondary Structure of TMDIV*. To further investigate the secondary structure and topography of TMDIV, the accessibility of R1 at each site along the segment to molecular $O_2$ and 70 mM NiEDDA was determined. $O_2$ is a nonpolar molecule that is preferentially soluble in the lipid phase while the polar NiEDDA is almost exclusively localized in the aqueous phase. Both reagents are excluded from packed protein regions. In a segment of secondary structure with anisotropic solvation, the accessibility to either reagent is periodic with a periodicity that reflects the type of secondary structure (*16*).

Figure 4a shows the sequence-specific variation in $\Pi(O_2)$ along TMDIV. Consistent with an α-helical configuration of the backbone, a periodicity of 3.6 is observed as demonstrated from the superimposed sinusoid. The oscillatory behavior continues uninterrupted along the sequence although a shift in the phase is detected near the last turn. Residues where R1 has the highest mobility correspond to local maxima in $\Pi(O_2)$. Thus, one face of the helix is solvated by the bilayer.

The opposite face of the helix has a complicated pattern of accessibility to NiEDDA. While a periodic pattern is observed in the 173−182 region, the periodicity is larger than 3.6. This might be the result of multiple protein contacts along the helix and implies a shift in the helix surface exposed to NiEDDA. Furthermore, a gradient of decreased accessibility is superimposed on the variations in Π. Along this stretch, the maxima in accessibility to NiEDDA occur near the minima of accessibility to $O_2$, indicating that this face of the helix is partly exposed to an aqueous environment. Between residues 182 and 189, the contrast is shallow, and the variations in the values of Π are within experimental error, indicating the loss of anisotropic solvation with respect to this probe. Because the accessibility is proportional to the product of the local concentration and the diffusion coefficient, it is possible that the diffusion of NiEDDA is restricted. If indeed TMDIV lines the translocation pathway, then some sort of physical barrier against passive diffusion is likely to exist. Consistent with this model, the immobilized line shape at residues 177, 181, 186, and 189 suggests a highly packed environment.

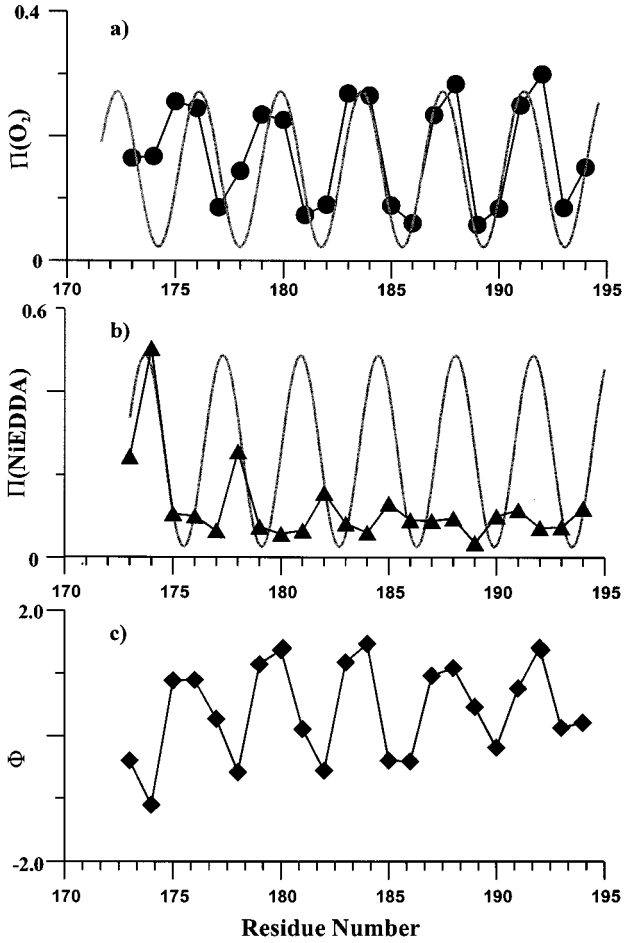


FIGURE 4: Accessibility parameters $\Pi(O_2)$ (panel a) and Π(NiEDDA) (panel b) and the depth parameter Φ (panel c) versus residue number. The gray trace in panels a and b is a sinusoid with a period of 3.6.

Figure 5 depicts a graphical representation of transmembrane domain IV, colored on the basis of the $O_2$ accessibility data. Thus, one face is exposed to the lipid bilayer (colored in blue), and the other face is oriented toward water (e.g., perhaps the aqueous translocation pathway) and/or other portions of the protein (colored in red). It should be noted that this model, which is based on the EPR data, (i) is in full agreement with our earlier predictions based on charged MTS reagent reactivity data (*21*) and (ii) permits extension of the α-helical structure to residue 173.

*Topography of TMDIV*. For a transmembrane helical segment, the periodic variations in accessibility to NiEDDA and $O_2$ are expected to be 180° out-of-phase as observed in Figure 4. Furthermore, the depth of selected sites should increase linearly toward the center of the bilayer. One approach to measure the depth of a nitroxide side chain is to calculate the parameter $\Phi = \ln [\Pi(O_2)/\Pi(\text{NiEDDA})]$ (*33*). For reagents of similar size or at highly exposed sites, Φ is independent of the local structure and is an increasing function of depth in the membrane.

However, the Φ values of R1 along the segment, shown in Figure 4c, did not display the expected linear increase as a function of residue number. In fact, the pattern of Figure 4 can be interpreted to suggest that the helix either lies parallel to the surface or is inserted at a shallow angle. Three lines of evidence argue against a parallel orientation of the helix.

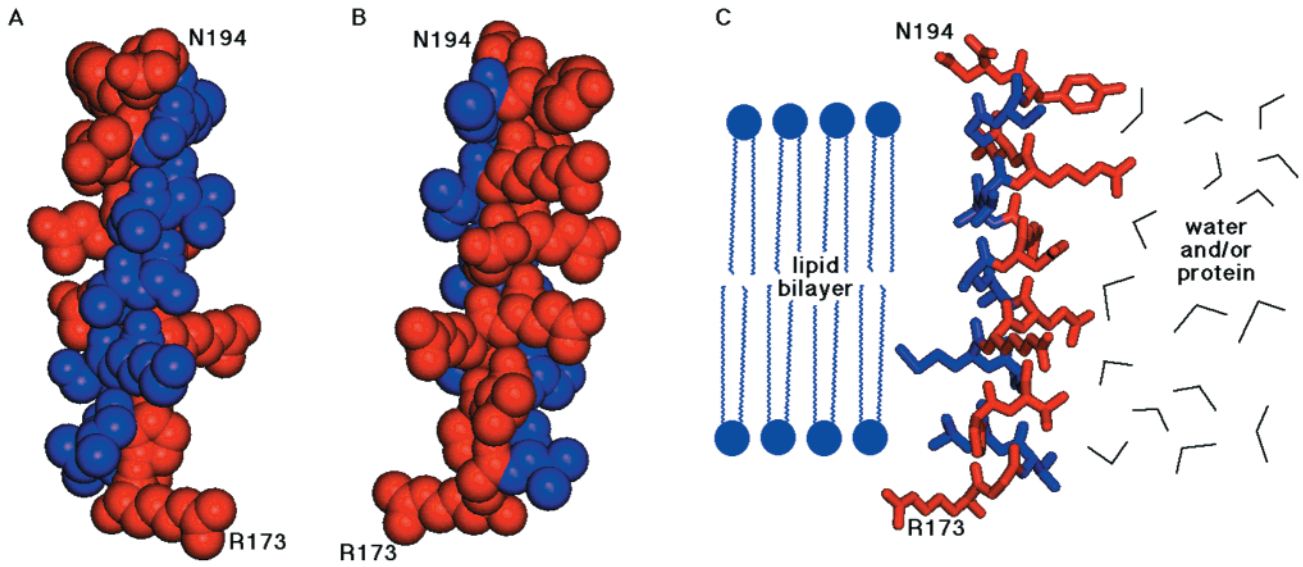


FIGURE 5: Transmembrane domain IV, colored according to the $O_2$ accessibility data. Blue indicates residues with high $O_2$ accessibility (interfacing with the lipid bilayer); red indicates low $O_2$ accessibility (interfacing with the aqueous translocation pathway and/or other domains within the CTP). Panel A: Space-filling representation of the portion of TMDIV which based on the EPR data is postulated to face the lipid bilayer. Panel B: Space-filling representation of TMDIV, rotated 180° around its *y*-axis, showing the residues which based on the EPR data are postulated to face away from the lipid bilayer and toward either an aqueous domain and/or other portions of the protein. Panel C: Stick figure representation of a side view of TMDIV, with a schematic representation of the lipid bilayer and the aqueous/protein interfaces included.

The regular decrease in the maxima of Π(NiEDDA) provides the first line of evidence for insertion of TMDIV in the membrane. If in fact the helix lies parallel to the surface, then all residues along one face of the helix should have similar values of Π(NiEDDA). Alternatively, if the gradient arises from the docking of a surface helix against the rest of the protein, then the chemical modification of cysteines 181 and 189 with charged moieties would have further destabilized the protein rather than restored activity. Comparison of the NiEDDA accessibilities of bilayer-facing residues with those of *n*-doxyl-phosphatidylcholines also provides an indication of depth. Figure 6 shows Π($O_2$), Π(NiEDDA) and Φ obtained for 5-, 7-, 10-, and 12-doxyl-phosphatidylcholine in bilayers containing Cys-less CTP at a lipid-to-protein ratio similar to that used for the R1-labeled mutants. It is noted that the minima in Π(NiEDDA) (i.e., residues facing the bilayer) along TMDIV have values similar to those of spin-labeled phospholipids at corresponding positions assuming a transmembrane configuration of TMDIV and using previously estimated values for the depths of spin labeled lipids (*34*). Residue 184 has NiEDDA accessibility similar to that of 12 spin-labeled phosphatidylcholine (i.e., approximately 16 Å).

The second line of evidence supporting a transmembrane disposition of this domain originates via comparison with other inner mitochondrial membrane transport proteins, where topography experiments utilizing several biochemical approaches indicate the homologous domain in other carriers is transmembranous (*35*−*37*).

The final and most direct evidence for a transmembrane configuration of TMDIV is obtained from the pattern of accessibility of the cysteine mutants to charged MTS reagents. Kaplan et al. (*21*) found that a gradient of decreasing accessibility is observed when charged MTS reagents are added from one side of the bilayer to proteoliposomes vectorially reconstituted. Furthermore, their data indicate that residues 181, 185, and 189 are readily accessible to charged reagents with reactivities that are 4−6 orders of magnitude faster than observed with lipid-exposed residues. This would not be the case if a parallel orientation of the helix is assumed with the polar face docked against the rest of the protein.

The accessibility of 181, 185, and 189 to charged reagents is not in contradiction with NiEDDA indicating increased protein order in that area. In comparing the two results, it is important to consider the vastly different time scale of the two experiments and the nature of the molecular event at the origin of each experimental parameter. Π(NiEDDA) is a measure of collision frequencies on the microsecond time scale, while MTS accessibilities are covalent reaction events occurring on the millisecond time scale.

What accounts for the apparent lack of increased depth along the lipid-exposed residues? In general, for a transmembrane helical segment, the oxygen accessibility will display in addition to the 3.6 periodicity a gradient of increasing accessibility that is symmetric with respect to the bilayer center. This is clearly not the case of TMDIV. Rather, a slight decrease of accessibility is observed in the 180−190 region, putatively localized near the center of the bilayer. Because the transporter is a dimer, one explanation is that the spatial organization of the dimer around the helix results in an excluded volume effect that lowers the diffusion coefficient of $O_2$. It is noted that the excluded volume is predicted to also lower Π(NiEDDA) to a larger extent. However, due to the poor solubility of NiEDDA in the bilayer, at the concentrations used in our experiments it may not be possible to discern this effect.

In conclusion, the present investigation demonstrates the feasibility of the site-directed spin labeling approach to study the mobility and accessibility of transmembrane domain

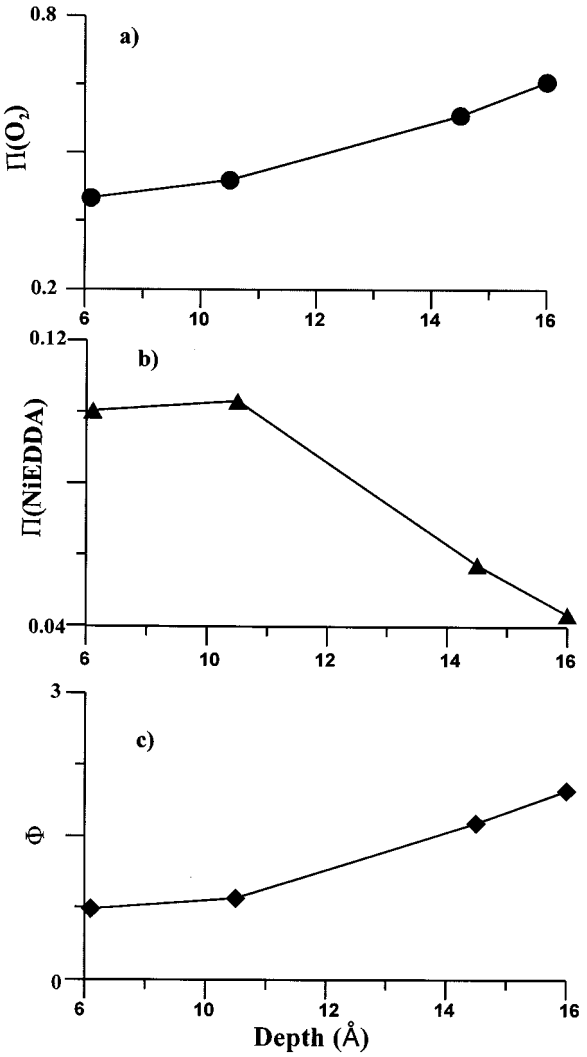


FIGURE 6: Accessibility parameters $\Pi(O_2)$ (panel a) and $\Pi$-(NiEDDA) (panel b) and the depth parameter $\Phi$ (panel c) for 5, 7, 10, and 12 spin-labeled phosphatidylcholine. Experiments were carried out utilizing liposomes containing the Cys-less CTP. Depth refers to the estimated depth (in Å) of the doxyl group from the lipid/water interface.

residues in the mitochondrial carrier family. In future studies, we plan to extend this approach (i) to study other transmembrane domains, (ii) to determine actual distance measurements between pairs of engineered cysteines, and (iii) to time-resolve substrate-induced conformational change at selected sites. In combination, these approaches should enable the molecular dissection of the CTP translocation mechanism.

## REFERENCES

1. Palmieri, F., Stipani, I., Quagliariello, E., and Klingenberg, M. (1972) *Eur. J. Biochem. 26*, 587−594.
2. Watson, J. A., and Lowenstein, J. M. (1970) *J. Biol. Chem. 245*, 5993−6002.
3. Endemann, G., Goetz, P. G., Edmond, J., and Brunengraber, H. (1982) *J. Biol. Chem. 257*, 3434−3440.
4. Brunengraber, H., and Lowenstein, J. M. (1973) *FEBS Lett. 36*, 130−132.
5. Conover, T. E. (1987) *Trends Biochem. Sci. 12*, 88−89.
6. Kaplan, R. S., Oliveira, D. L., and Wilson, G. L. (1990) *Arch. Biochem. Biophys. 280*, 181−191.
7. Kaplan, R. S., Mayor, J. A., Blackwell, R., Maughon, R. H., and Wilson, G. L. (1991) *Arch. Biochem. Biophys. 287*, 305−311.
8. Kaplan, R. S., Mayor, J. A., Johnston, N., and Oliveira, D. L. (1990) *J. Biol. Chem. 265*, 13379−13385.
9. Bisaccia, F., De Palma, A., and Palmieri, F. (1989) *Biochim. Biophys. Acta 977*, 171−176.
10. Kaplan, R. S., Mayor, J. A., and Wood, D. O. (1993) *J. Biol. Chem. 268*, 13682−13690.
11. Xu, Y., Mayor, J. A., Gremse, D., Wood, D. O., and Kaplan, R. S. (1995) *Biochem. Biophys. Res. Commun. 207*, 783−789.
12. Kaplan, R. S., Mayor, J. A., Gremse D. A., and Wood, D. O. (1995) *J. Biol. Chem. 270*, 4108−4114.
13. Xu, Y., Kakhniashvili, D. A., Gremse, D. A., Wood, D. O., Mayor, J. A., Walters, D. E., and Kaplan, R. S. (2000) *J. Biol. Chem. 275*, 7117−7124.
14. Kotaria, R., Mayor, J. A., Walters, D. E., and Kaplan, R. S. (1999) *J. Bioenerg. Biomembr. 31*, 543−549.
15. Hubbell, W. L., Mchaourab, H. S., Altenbach, C., and Lietzow, M. A. (1996) *Structure 4*, 779−783.
16. Hubbell, W. L., Gross, A., Langen, R., and Lietzow, M. A. (1998) *Curr. Opin. Struct. Biol. 8*, 649−656.
17. Koteiche, H. A., Berengian, A. R., and Mchaourab, H. S. (1998) *Biochemistry 37*, 12681−12688.
18. Farrens, D. L., Altenbach, C., Yang, K., Hubbell, W. L., and Khorana, H. G. (1996) *Science 274*, 768−770.
19. Voss, J., He, M. M., Hubbell, W. L., and Kaback, H. R. (1996) *Biochemistry 35*, 12915−12918.
20. Sun, J., Voss, J., Hubbell, W. L., and Kaback, H. R. (1999) *Biochemistry 38*, 3100−3105.
21. Kaplan, R. S., Mayor, J. A., Brauer, D., Kotaria, R., Walters, D. E., and Dean, A. M., (2000) *J. Biol. Chem. 275*, 12009−12016.
22. Farahbakhsh, Z. T., Altenbach, C., and Hubbell, W. L. (1992) *Photochem. Photobiol. 56*, 1019−1033.
23. Kaplan, R. S., and Pedersen, P. L. (1985) *Anal. Biochem. 150*, 97−104.
24. Thorgeirsson, T. E., Russell, C. J., King, D. S., and Shin, Y. K. (1996) *Biochemistry 35*, 1803−1809.
25. Bolin K. A., Hanson, P., Wright, S. J., and Millhauser, G. L. (1998) *J. Magn. Reson. 131*, 248−253.
26. Hubbell, W. L., and Altenbach, C. (1994) *Curr. Opin. Struct. Biol. 4*, 566−573.
27. Altenbach, C., Marti, T., Khorana, H. G., and Hubbell, W. L. (1990) *Science 248*, 1088−1092.
28. Mchaourab, H. S., Lietzow, M. A., Hideg, K., and Hubbell, W. L. (1996) *Biochemistry 35*, 7692−7704.
29. Altenbach, C., Yang, K., Farrens, D. L., Farahbakhsh, Z. T., Khorana, H. G., and Hubbell, W. L. (1996) *Biochemistry 35*, 12470−12478.
30. Freed, J. H., and Schneider, D. J. (1989) in *Biological Magnetic Resonance, Vol. 8, Spin Labeling Theory and Applications* (Berliner, L. J., and Reuben, J., Ed.) pp 1−76, Plenum Press, New York.
31. Mchaourab H. S., Kalai T., Hideg K., and Hubbell W. L. (1999) *Biochemistry 38*, 2947−2955.
32. Mchaourab, H. S., Oh, K. J., Fang, C. J., and Hubbell, W. L. (1997) *Biochemistry 36*, 307−316.
33. Altenbach, C., Greenhalgh, D. A., Khorana, H. G., and Hubbell, W. L. (1994) *Proc. Natl. Acad. Sci. U.S.A. 91*, 1667−1671.
34. Dalton, L. A., McIntyre, J. O., and Fleischer, S. (1987) *Biochemistry 26*, 2117−2130.
35. Miroux, B., Frossard, V., Raimbault, S., Ricquier, D., and Bouillaud, F. (1993) *EMBO J. 12*, 3739−3745.
36. Klingenberg, M. (1989) *Arch. Biochem. Biophys. 270*, 1−14.
37. Palmieri, F. (1994) *FEBS Lett. 346*, 48−54.

BI000433E